Journal of Solid State Chemistry 215 (2014) 245–252

Contents lists available at ScienceDirect

Journal of Solid State Chemistry

journal homepage: www.elsevier.com/locate/jssc

$Pb_5Fe_3TiO_{11}Cl$: A rare example of Ti(IV) in a square pyramidal oxygen coordination

Maria Batuk [a,*], Dmitry Batuk [a], Artem M. Abakumov [a,b], Joke Hadermann [a]

[a] Electron Microscopy for Materials Research (EMAT), University of Antwerp, Groenenborgerlaan 171, B-2020 Antwerp, Belgium
[b] Department of Chemistry, Moscow State University, 119991 Moscow, Russia

ARTICLE INFO

Article history:
Received 20 February 2014
Received in revised form
2 April 2014
Accepted 3 April 2014
Available online 12 April 2014

Keywords:
Perovskite
Oxychloride
Scanning transmission electron microscopy
Atomic resolution EDX
Neutron powder diffraction
Five-fold coordinated titanium

ABSTRACT

A new oxychloride $Pb_5Fe_3TiO_{11}Cl$ has been synthesized using the solid state method. Its crystal and magnetic structure was investigated in the 1.5–550 K temperature range using electron diffraction, high angle annular dark field scanning transmission electron microscopy, atomic resolution energy dispersive X-ray spectroscopy, neutron and X-ray powder diffraction. At room temperature $Pb_5Fe_3TiO_{11}Cl$ crystallizes in the *P*4/*mmm* space group with the unit cell parameters $a=3.91803(3)$ Å and $c=19.3345(2)$ Å. $Pb_5Fe_3TiO_{11}Cl$ is a new $n=4$ member of the oxychloride perovskite-based homologous series $A_{n+1}B_nO_{3n-1}Cl$. The structure is built of truncated $Pb_3Fe_3TiO_{11}$ quadruple perovskite blocks separated by CsCl-type Pb_2Cl slabs. The perovskite blocks consist of two layers of $(Fe,Ti)O_6$ octahedra sandwiched between two layers of $(Fe,Ti)O_5$ square pyramids. The Ti^{4+} cations are preferentially located in the octahedral layers, however, the presence of a noticeable amount of Ti^{4+} in a five-fold coordination environment has been undoubtedly proven using neutron powder diffraction and atomic resolution compositional mapping. $Pb_5Fe_3TiO_{11}Cl$ is antiferromagnetically ordered below 450(10) K. The ordered Fe magnetic moments at 1.5 K are 4.06(4) μ_B and 3.86(5) μ_B on the octahedral and square-pyramidal sites, respectively.

1. Introduction

The crystal structure of the mineral hematophanite $Pb_4Fe_3O_8Cl$ can be represented as an alternation of incomplete perovskite $Pb_4Fe_3O_8$ blocks with layers of chlorine atoms (Fig. 1) [1–4]. Each perovskite block is built of one layer of FeO_6 octahedra sandwiched between layers of FeO_5 square pyramids, forming a slab with a thickness of $3a_p$ ($a_p \approx 4.0$ Å is the perovskite lattice parameter). Recently, we have demonstrated that the thickness of the perovskite block in the hematophanite $Pb_4Fe_3O_8Cl$ structure can be increased up to two and three octahedral layers resulting in the $Pb_4BiFe_4O_{11}Cl$ and $Pb_4Bi_2Fe_5O_{14}Cl$ compounds, respectively [5]. Structures with different thicknesses of the perovskite blocks form a homologous series with the general formula $A_{n+1}B_nO_{3n-1}Cl$ ($n=2$–5; A=Pb, Ba, Sr; B=Fe, Cu, Nb, Ta, Sb, Ru) [5–14]. According to the neutron powder diffraction study, both hematophanite ($n=3$) and the successive member of the series $Pb_4BiFe_4O_{11}Cl$ ($n=4$) demonstrate a G-type antiferromagnetic arrangement of the Fe magnetic moments with very close Néel temperatures $T_N \sim 600$ K [4,5].

As it was illustrated for other homologous series, the thickness of the perovskite blocks (e.g., n in $A_{n+1}B_nO_{3n-1}Cl$) can be increased through a heterovalent replacement on the B sublattice, for example, via the Ti^{4+} for Fe^{3+} substitution [15,16]. In this paper we report on a new $n=4$ member of the $A_{n+1}B_nO_{3n-1}Cl$ series with the $Pb_5Fe_3TiO_{11}Cl$ composition. The crystal and magnetic structure of the new compound was studied in a temperature range of 1.5–550 K using a combination of transmission electron microscopy techniques and neutron powder diffraction. $Pb_5Fe_3TiO_{11}Cl$ represents a system with a partial Ti^{4+}/Fe^{3+} cation ordering driven by their specific coordination preferences.

2. Experimental part

Samples of $Pb_5Fe_3TiO_{11}Cl$ were synthesized by a solid-state reaction of PbO (Sigma-Aldrich, $>99.9\%$), $PbCl_2$ (Aldrich, 99.98%), TiO_2 (Aldrich, $\geq 99.5\%$, nanopowder with ≈ 21 nm particle size) and Fe_2O_3 (Aldrich, nanopowder with <50 nm particle size) in air. The starting materials were weighed, thoroughly ground under acetone and pressed into pellets. The pellets were annealed in two steps: at 670 °C for 10 h and at 800 °C for 20 h with intermediate regrinding.

* Corresponding author. Tel.: +32 32653695; fax: +32 32653257.
E-mail address: Maria.Batuk@uantwerpen.be (M. Batuk).

http://dx.doi.org/10.1016/j.jssc.2014.04.002
0022-4596/

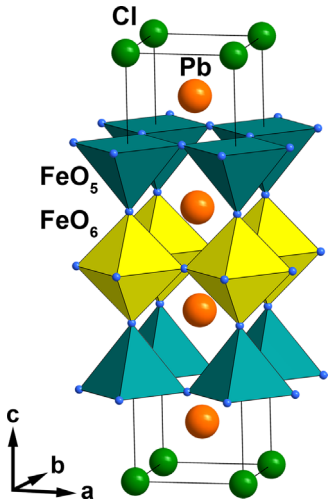

Fig. 1. Crystal structure of hematophanite $Pb_4Fe_3O_8Cl$.

The phase purity of the samples was verified using the X-ray powder diffraction (XPD) data recorded on a Huber G670 Guinier diffractometer (Cu$K\alpha_1$-radiation, curved Ge(111) monochromator, transmission mode, image plate). The chemical composition was confirmed by the energy dispersive X-ray (EDX) analysis, which was conducted with a JEOL 5510 scanning electron microscope (SEM) equipped with an INCAx-sight 6587 system (Oxford instruments). The EDX spectra from about 60 crystallites were collected, and the Pb–M, Fe–K, Ti–K, and Cl–K absorption edges were used to determine the elemental ratio.

Neutron powder diffraction (NPD) data were collected with the high-resolution powder diffractometer HRPT at the Laboratory for Neutron Scattering of the Paul Scherrer Institute (LNS PSI, Villigen, Switzerland) [17]. The data were collected at the wavelength $\lambda = 1.8857$ Å in the 2θ range of 8–160°. The sample (~15 g) was placed in a vanadium container with a diameter of 10 mm. The measurements were conducted in the temperature range from 1.5 to 550 K with a step of 50 K. The data from 1.5 to 300 K were obtained using an ILL ^{4}He flow cryostat. High-temperature measurements were performed using a custom-built tantalum radiation furnace. The symmetry analysis of possible magnetic configurations has been carried out with the program BasIreps. The crystal and magnetic structures were refined using the FULLPROF program package [18].

Electron diffraction (ED) patterns were obtained using a FEI Tecnai G2 (200 kV) microscope. High-angle annular dark-field scanning transmission electron microscopy (HAADF-STEM) and EDX-STEM experiments were conducted using a FEI Titan 80-300 "cubed" microscope equipped with a Super-X detector and operated at 200 kV. The results were recorded using probes with convergence semi-angles in the 21–25 mrad range (with a probe size of about 1 Å). The probe current ranged between 50 and 200 pA. Samples for the TEM study were prepared by grinding the material under ethanol and depositing a few drops of the suspension onto holey carbon grids. The simulated HAADF-STEM images were calculated using the QSTEM 2.0 software [19]. The calculated electron diffraction patterns were obtained using the JEMS software.

3. Results

3.1. Crystal structure of $Pb_5Fe_3TiO_{11}Cl$

The composition of the sample determined from the EDX-SEM measurements is $Pb_{4.9(2)}Fe_{2.9(1)}Ti_{1.1(1)}O_xCl_{1.1(2)}$, which is close to the nominal composition $Pb_5Fe_3TiO_{11}Cl$. The room-temperature XPD pattern after the Le Bail fitting is shown in Fig. 2. It can be completely indexed on a tetragonal lattice with the space group $P4/mmm$ and the cell parameters $a = 3.91803(3)$ Å $\approx a_p$ and $c = 19.3345(2)$ Å $\approx 5a_p$. The electron diffraction patterns of $Pb_5Fe_3TiO_{11}Cl$ (Fig. 3) are indexed in the $P4/mmm$ unit cell, consistent with the XPD data. No reflection conditions appear on the ED patterns taken along the main zone axes, confirming the $P4/mmm$ space group. However, in the [310] ED pattern there are lines of a modulated diffuse intensity propagating along the c^*-direction (marked with arrows in Fig. 3). These lines originate from a local ordering of the BO_6 octahedra rotations about the c-axis, as will be discussed below.

The crystal structure of $Pb_5Fe_3TiO_{11}Cl$ was refined using the Rietveld method from NPD data collected in the temperature range from 1.5 to 550 K. The diffuse intensity due to the local ordering does not noticeably contribute to the NPD patterns and therefore only the average structure with the space group $P4/mmm$ has been considered for the refinement. The structural model was constructed using the building principles of the $A_{n+1}B_nO_{3n-1}Cl$ homologous series [5]. Due to the large difference between the Fe and Ti scattering lengths (0.945 and −0.344 fm, respectively), the occupancy factors of Fe and Ti could be refined with a high accuracy. At $T = 550$ K the refinement converged to the occupancy factors $g_P = 0.889(5)Fe + 0.111(5)Ti$ at the square-pyramidal (P) site (the FeTi1 position) and $g_O = 0.617(5)Fe + 0.383(5)Ti$ at the octahedral (O) site (the FeTi2 position) with the total composition $Pb_5Fe_{3.01(1)}Ti_{0.99(1)}O_{11}Cl$. Since it is very close to the nominal composition $Pb_5Fe_3TiO_{11}Cl$, the Fe and Ti occupancies were rounded off and fixed as $g_P = 0.89Fe + 0.11Ti$ in the FeTi1 site and $g_O = 0.61Fe + 0.39Ti$ in the FeTi2 site. These values were used for the crystal structure refinement at other temperatures. An attempt to place Ti only in the octahedral FeTi2 position led to a highly negative isotropic atomic displacement parameter (U_{iso}) for the FeTi2 position. The presence of Ti in square pyramidal coordination was additionally confirmed by atomic resolution STEM-EDX analysis (see below).

The atomic displacement parameter of the O2 atom forming the basal square plane of the (Fe,Ti)O_6 octahedra was found to be noticeably higher than that of the other oxygen atoms (0.046 Å^2 at $T = 1.5$ K). The splitting of the O2 position along the a-direction reduces the displacement parameter (to 0.025 Å^2), bringing it closer to the values of other oxygen positions. Such displacement indicates disordered rotations of the (Fe,Ti)O_6 octahedra about the c-axis. This is very typical for the layered perovskite-based structures, including hematophanite and $Pb_4BiFe_4O_{11}Cl$ [4,5].

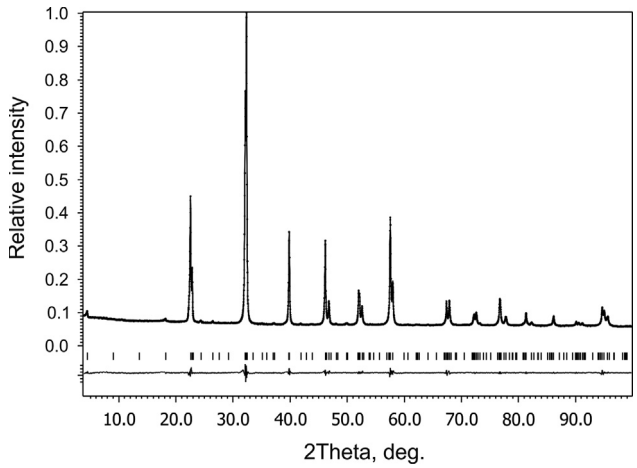

Fig. 2. Experimental, calculated and difference XPD profiles of $Pb_5Fe_3TiO_{11}Cl$ after the Le Bail fit.

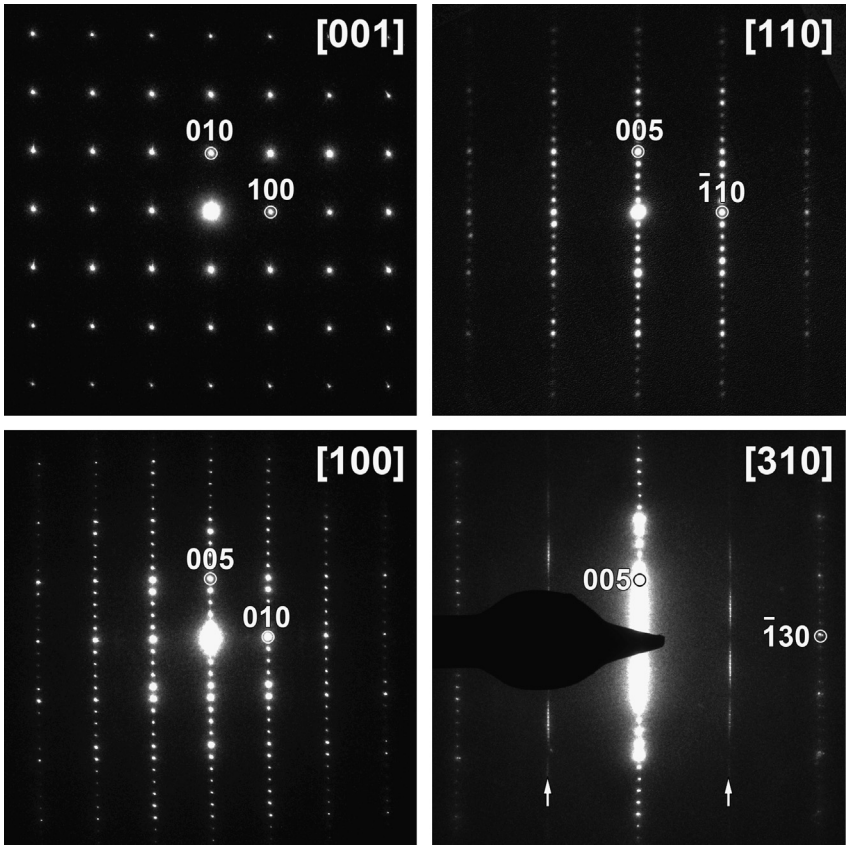

Fig. 3. Electron diffraction patterns of $Pb_5Fe_3TiO_{11}Cl$. The diffuse intensity lines in the [310] ED pattern are marked with arrows.

Table 1
Selected parameters of the Rietveld refinements of $Pb_5Fe_3TiO_{11}Cl$.

Formula	$Pb_5Fe_3TiO_{11}Cl$		
Space group	*P4/mmm*		
T, K	1.5	300	550
a, Å	3.90348(5)	3.91542(6)	3.93380(6)
c, Å	19.2641(4)	19.3216(4)	19.3996(4)
Z	1		
Cell volume, $Å^3$	293.53(1)	296.21(1)	300.20(1)
Calculated density, g/cm^3	8.28	8.20	8.09
M(Fe1), μ_B	4.06(4)	3.03(5)	–
M(Fe2), μ_B	3.86(5)	2.74(6)	–
Radiation	Neutron, $\lambda = 1.8857$ Å		
Parameters refined	34	34	32
R_F, R_P, R_{wP}	0.021, 0.050, 0.067	0.020, 0.045, 0.061	0.025, 0.042, 0.056

The parameters of the Rietveld refinement at 1.5, 300 and 550 K are listed in Table 1. The fractional atomic coordinates and the atomic displacement parameters are provided in Table 2, the selected bond lengths are in Table 3. The experimental, calculated and difference NPD profiles after the refinements at 1.5, 300 and 550 K are given in Fig. 4. The refined room-temperature crystal structure is shown in Fig. 5.

The temperature evolution of the $Pb_5Fe_3TiO_{11}Cl$ structure is very similar to that of $Pb_4BiFe_4O_{11}Cl$ [5] and hematophanite $Pb_4Fe_3O_8Cl$ [4]. Upon heating from 1.5 to 550 K the structure slightly expands by $\approx 0.8\%$ and $\approx 0.7\%$ in the *a* and *c* directions, respectively (Fig. S1 of the Supporting Information). The increase in the *c* cell parameter is mainly related to the expansion of the Pb_2Cl slab, whereas the configuration of the perovskite blocks does not noticeably change in the whole temperature range. The thickness of this slab can be measured by the Pb1–Pb1 distance (Fig. S2 of the Supporting Information). The rotation angle of the $(FeTi2)O_6$ octahedra decreases with temperature from 7.33(2)° at 1.5 K to 3.54(2)° at 550 K. These values are smaller in comparison with both $Pb_4BiFe_4O_{11}Cl$ (8.4° at 1.5 K to 7.6° at 700 [5]) and $Pb_4Fe_3O_8Cl$ (12.8° at 10 K and 10.3° at 650 K [4]).

3.2. Magnetic structure of $Pb_5Fe_3TiO_{11}Cl$

Below 450 K the material is antiferromagnetically (AFM) ordered. Magnetic reflections appear on the NPD patterns and their intensities systematically grow upon cooling. The magnetic reflections can be indexed with the propagation vector $\mathbf{k}=(1/2, 1/2,0)$. The model of the magnetic structure was expected to be similar to that of hematophanite and $Pb_4BiFe_4O_{11}Cl$ with the Fe magnetic moments ordered antiferromagnetically along all three crystallographic directions with spins lying perpendicular to the

Table 2
Atomic parameters of $Pb_5Fe_3TiO_{11}Cl$ from the Rietveld refinement against neutron powder diffraction data at 1.5, 300 and 550 K.

Atom	Site	(*x*,*y*,*z*)		1.5 K	300 K	550 K
Pb1	2*h*	1/2,1/2,*z*	U_{iso}, Å^2	0.009(1)	0.017(1)	0.015(1)
			z	0.0941(1)	0.0950(1)	0.0956(1)
Pb2	2*h*	1/2,1/2,*z*	U_{iso}, Å^2	0.015(1)	0.025(1)	0.027(1)
			z	0.3029(2)	0.3031(2)	0.3033(2)
Pb3	1*d*	1/2,1/2,1/2	U_{iso}, Å^2	0.017(1)	0.031(1)	0.034(1)
FeTi1[a]	2*g*	0,0,*z*	U_{iso}, Å^2	0.006(1)	0.013(1)	0.010(1)
			z	0.1946(2)	0.1945(2)	0.1948(2)
FeTi2[b]	2*g*	0,0,*z*	U_{iso}, Å^2	0.004(1)	0.007(1)	0.006(1)
			z	0.3960(3)	0.3967(3)	0.3970(3)
Cl	1*a*	0,0,0	U_{iso}, Å^2	0.017(1)	0.032(1)	0.042(1)
O1	4*i*	0,1/2,*z*	U_{iso}, Å^2	0.010(1)	0.015(1)	0.015(1)
			z	0.1660(1)	0.1664(1)	0.1667(1)
O2	8*t*	*x*,1/2,*z*	U_{iso}, Å^2	0.025(1)	0.029(1)	0.028(1)
			x	0.064(2)	0.052(2)	0.031(3)
			z	0.3919(2)	0.3925(2)	0.3927(2)
O3	2*g*	0,0,*z*	U_{iso}, Å^2	0.012(1)	0.020(1)	0.021(1)
			z	0.2881(2)	0.2886(2)	0.2889(2)
O4	1*b*	0,0,1/2	U_{iso}, Å^2	0.014(2)	0.021(2)	0.022(2)

[a] Occupancy 0.89Fe+0.11Ti.
[b] Occupancy 0.61Fe+0.39Ti.

Table 3
Selected interatomic distances of $Pb_5Fe_3TiO_{11}Cl$ from the Rietveld refinement against neutron powder diffraction data at 1.5 , 300 and 550 K.

Bond	1.5 K	300 K	550 K
Pb1–O1 × 4	2.393(2)	2.394(2)	2.403(2)
Pb1–Cl × 4	3.302(1)	3.322(2)	3.343(2)
Pb2–O2 × 2	2.416(5)	2.463(6)	2.532(9)
Pb2–O2 × 2	2.792(5)	2.766(7)	2.715(10)
Pb2–O3 × 4	2.775(1)	2.783(1)	2.796(1)
Pb3–O2 × 4	2.689(5)	2.719(6)	2.782(8)
Pb3–O2 × 4	3.031(5)	2.997(6)	2.949(9)
Pb3–O4 × 4	2.760(1)	2.769(1)	2.782(1)
FeTi1–O1 × 4	2.028(1)	2.032(1)	2.041(1)
FeTi1–O3	1.801(5)	1.818(5)	1.826(5)
FeTi2–O2 × 4	1.969(1)	1.970(1)	1.972(1)
FeTi2–O3	2.079(7)	2.089(7)	2.097(7)
FeTi2–O4	2.003(6)	1.996(6)	1.998(6)

c-axis [4,5]. Using the determined propagation vector, we have performed the group theory symmetry analysis of the possible magnetic structures. There are two symmetry-independent magnetic iron atoms per unit cell in the structure: Fe1 in the square-pyramidal position and Fe2 in the octahedral position. Since the magnetic peak intensities increase smoothly on cooling, it was assumed that both the Fe1 and Fe2 magnetic ions order with just one irreducible representation (irrep), which is the same for both positions. The basis vectors (BV) of the irreps contributing to the magnetic representation for both sites with nonzero coefficients are given in Table S1 of the Supporting Information. Among these irreps only two-dimensional Γ_9 and Γ_{10} representations provide the structures with Fe magnetic moments that lie within the *ab*-plane. Both irreps were tried for the Rietveld refinement; the Γ_9 led to a noticeably lower *R* factor. It should be noted that the magnetic symmetry allows any arbitrary orientation of the magnetic moments within the *ab*-plane, providing identical fits to the NPD pattern. Thus, the exact orientation of the magnetic moments cannot be determined from the NPD experiment and therefore the magnetic moments were fixed along the diagonal of the *ab* unit cell face. The refined magnetic structure is shown in Fig. 6. The magnetic structures with the moments aligned along the *c*-axis were also tested and discarded as unsatisfactory.

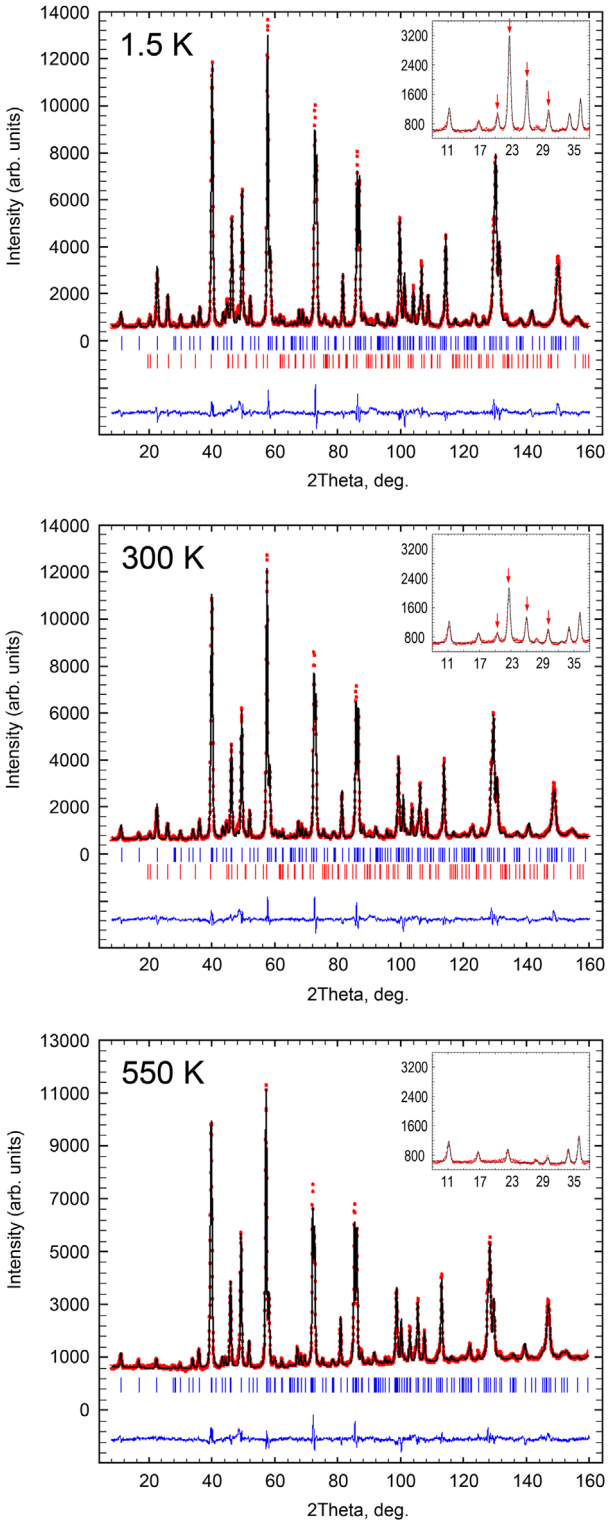

Fig. 4. Experimental, calculated and difference NPD profiles of $Pb_5Fe_3TiO_{11}Cl$ after the Rietveld refinement at 1.5, 300 and 550 K. The upper (blue) set of reflection markers refers to the nuclear structure, the bottom (red) to the magnetic structure. The insets show the enlarged low-angle region, where the magnetic reflections are marked with arrows. (For interpretation of the references to color in this figure legend, the reader is referred to the web version of this article.)

The values of the ordered magnetic moments obtained at 1.5 K are 4.06(4) and 3.86(5) μ_B per Fe ion in the Fe1 and Fe2 sites, respectively. Although, these values are lower than the expected magnetic moment of 5 μ_B for the high spin Fe^{3+}, they are in the same range as determined for $Pb_4Fe_3O_8Cl$ (3.94(3) μ_B) [4] and

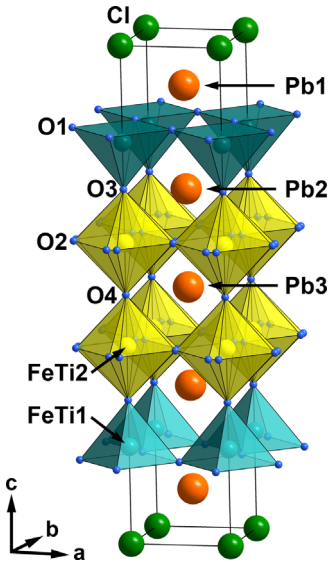

Fig. 5. The room-temperature structure of $Pb_5Fe_3TiO_{11}Cl$. The O2 positions are split due to the disorder in the rotations of the $(FeTi2)O_6$ octahedra.

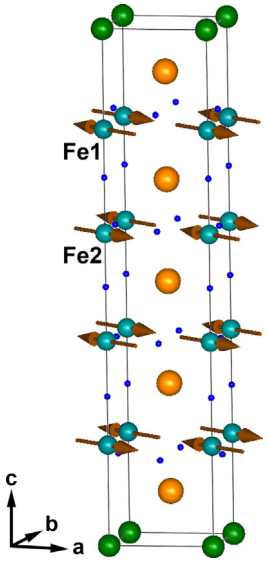

Fig. 6. The magnetic structure of $Pb_5Fe_3TiO_{11}Cl$ at 1.5 K (Fe atoms are shown as blue spheres, Cl – green, Pb – orange, O – dark blue). The Fe1 and Fe2 spins are oriented along the *ab*-diagonal. (For interpretation of the references to color in this figure legend, the reader is referred to the web version of this article.)

$Pb_4BiFe_4O_{11}Cl$ (3.93(3) and 3.62(4) μ_B) [5]. Such a decrease of the Fe^{3+} saturated magnetic moment in these structures might be explained by the strong covalent interaction between the Fe 3*d* orbitals and the O 2*p* orbitals, which leads to a reduction of the magnetic neutron scattering form factor of Fe [20–22]. The temperature dependence of the ordered magnetic moments $M(T)$ is shown in Fig. 7. The experimental data can be fitted with the phenomenological formula $M(T)=M_0[1-(T/T_N)^{\alpha}]^{\beta}$, where M_0 is the saturated magnetic moment at 0 K, T_N is the Néel temperature, β is the critical exponent, α is an empirical parameter [23–25]. The fitting parameters are: $T_N=450(10)$ K, $\beta=0.38(3)$, $\alpha=1.5(2)$, $M_0(Fe1)=4.15(4)\ \mu_B$, $M_0(Fe2)=3.86(4)\ \mu_B$. The obtained Néel temperature of 450(10) K is noticeably lower than that of hematophanite (602 K [2] or 610(5) K [4]) and $Pb_4BiFe_4O_{11}Cl$ (595(17) K [5]) due to the dilution of the magnetic lattice by a non-magnetic cation Ti^{4+}. The low temperature saturated magnetic moments M_0 are close to the magnetic moments refined at 1.5 K. The estimated value of $\beta=0.38$

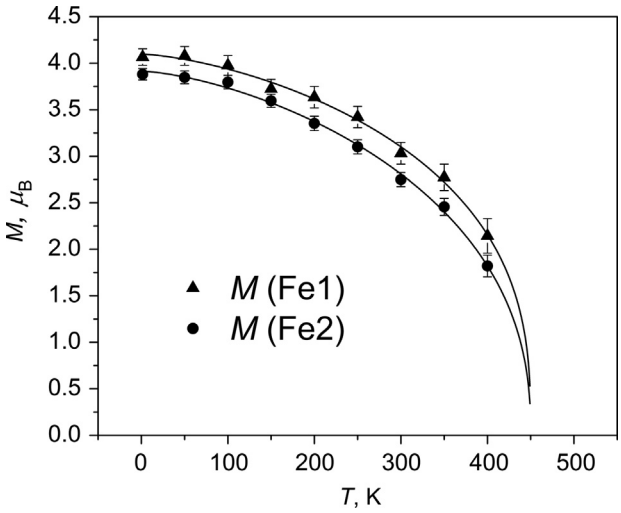

Fig. 7. Temperature dependence of ordered magnetic moments for Fe1 and Fe2. The data are fitted with the $M=M_0(1-(T/T_N)^{\alpha})^{\beta}$ empirical function.

(3) is close but slightly higher than the theoretically predicted values for the three-dimensional systems (0.32, 0.33 or 0.36 for the Ising, *XY* and Heisenberg models, respectively) [26]. However, it should be noted that the β critical exponent should be determined from a temperature range close to the transition temperature. In our case β was calculated by the extrapolation of the experimental data in the wide temperature range 1.5–450 K as we do not have enough experimental points in the interval close to T_N.

3.3. HAADF-STEM imaging and atomic resolution EDX mapping

The crystal structure solution was confirmed by the HAADF-STEM imaging. An experimental HAADF-STEM image of $Pb_5Fe_3TiO_{11}Cl$ taken along the most informative [100] zone axis is shown in Fig. 8. The brightest dots are attributed to the Pb columns ($Z_{Pb}=82$). They form a square pattern with a spacing of ≈ 3.9 Å between the dots and correspond to the *A* positions of the perovskite structure. The (Fe,Ti)–O columns appear as weaker dots ($Z_{Fe}=26$, $Z_{Ti}=22$, $Z_O=8$). The periodically occurring dark stripes (marked by arrowheads in Fig. 8) are attributed to the layers of chlorine atomic columns ($Z_{Cl}=17$). The room temperature structural data were used for the HAADF-STEM image simulations. The calculated image shown as an inset in Fig. 8 is attributed to the crystal thickness of 8 nm and is in a good agreement with experimental one.

Fig. 9 represents the atomic resolution elemental maps of Pb, Fe, Ti, O and Cl together with the mixed Fe/Ti map and the corresponding Fe/Ti intensity profile. The EDX signal profiles for Fe and Ti were fitted with a set of Gaussian functions with equal half width of all peaks [27]. The Fe and Ti EDX maps and the fits of the intensity profiles clearly demonstrate that Ti is preferentially situated in the octahedral FeTi2 position, but there is also a noticeable amount of Ti located in the square pyramidal FeTi1 position, in agreement with the occupancy factors refined from the NPD data. Two more elemental maps can be found in the Supporting Information (Figs. S3 and S4).

Several crystals with planar defects were observed in the sample as well. An example is given in Fig. 10. It corresponds to the random insertion of lamellae with $n=3$ (hematophanite) structure in a matrix of the $n=4$ structure. This type of defects is very common for layered perovskite-based structures. Elemental maps from an area with defects are shown in Fig. 11. According to the Fe/Ti mixed map and the corresponding intensity profile, Ti occupies octahedral and pyramidal positions not only in the

$Pb_5Fe_3TiO_{11}Cl$ structure, but also in the hematophanite type of structure. However, the amount of Ti in the hematophanite block is significantly smaller and most of the Ti is concentrated at the central octahedral layer of this block.

4. Discussion

$Pb_5Fe_3TiO_{11}Cl$, a new $n=4$ member of the $A_{n+1}B_nO_{3n-1}Cl$ homologous series, was synthesized in a single phase form using the solid state technique. Whereas in another $n=4$ member $Pb_4BiFe_4O_{11}Cl$ [5] the B positions are occupied by the Fe^{3+} only, in $Pb_5Fe_3TiO_{11}Cl$ 25% of the B positions are occupied by Ti^{4+}. Fe^{3+} and Ti^{4+} tend to be partially ordered in different layers with the occupancy $g_P=0.89Fe+0.11Ti$ in the square-pyramidal FeTi1 site and $g_O=0.61Fe+0.39Ti$ in the octahedral FeTi2 site (see Fig. 5). The layered ordering of the B-cations in perovskites is extremely rare if it is not coupled to the simultaneous ordering of the oxygen atoms and vacancies [28,29]. Typically the layered B/B' cation ordering in perovskites requires the charge difference $\Delta q=2$ and should be stabilized by a first order Jahn–Teller distortion of the $B'O_6$ octahedra [28]. Both conditions are definitely not fulfilled in $Pb_5Fe_3TiO_{11}Cl$. The tendency of Ti^{4+} to order with Fe^{3+} can be explained by the preference for a different coordination environment: for the Ti^{4+} cations the octahedral coordination is more typical, whereas the five-fold coordination is uncommon. Among a few known structures with five-coordinated titanium are the mineral fresnoite ($Ba_2TiSi_2O_8$) [30], several compounds related to fresnoite ($Sr_2TiSi_2O_8$, $Ba_2TiGe_2O_8$ [31], $Na_4Ti_2Si_8O_{22}\cdot 4H_2O$ [32]), metatitanates of alkaline metals ($MNaTiO_3$, where M=K [33], Rb or Cs [34]) and a recently published Sm_2TiO_5 [35]. Also one can mention chalcogenides $Ln_2Ti_2S_2O_5$ (Ln=Nd, Pr, Sm) [36] and

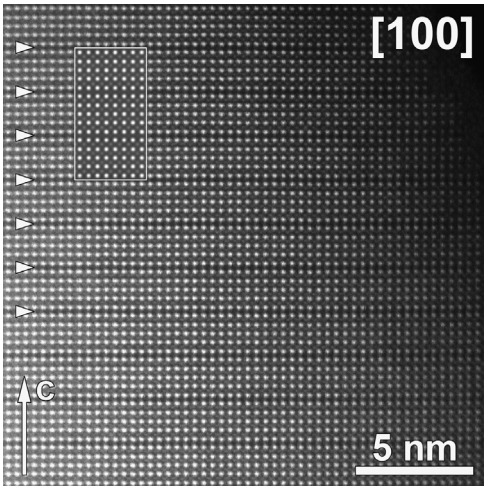

Fig. 8. HAADF-STEM image of $Pb_5Fe_3TiO_{11}Cl$ taken along the [100] zone axis. Arrowheads indicate the chlorine layers. The inset shows the simulated image calculated using the structural parameters refined from the NPD data.

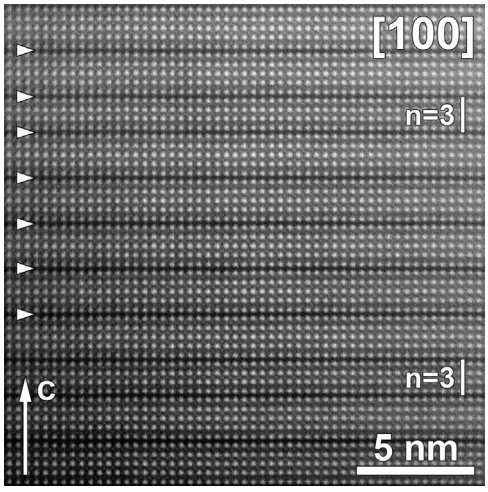

Fig. 10. [100] HAADF-STEM image, showing defects observed in $Pb_5Fe_3TiO_{11}Cl$: $n=3$ lamellae are randomly inserted in the $n=4$ matrix. Arrowheads indicate the chlorine layers.

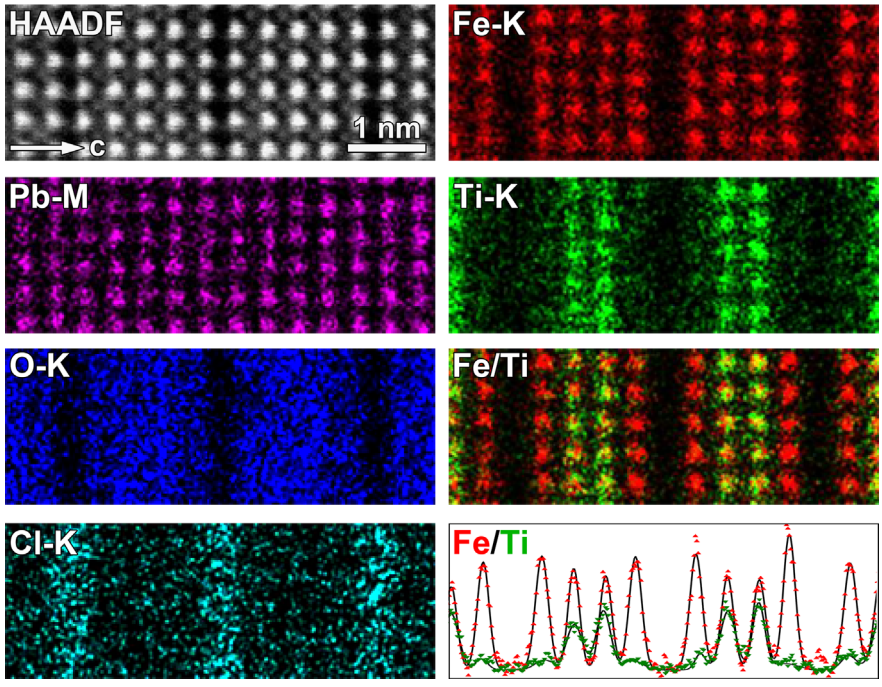

Fig. 9. High resolution HAADF-STEM image (upper corner) of $Pb_5Fe_3TiO_{11}Cl$ taken along the [100] zone axis, individual Pb, Fe, Ti, O and Cl atomic EDX elemental maps, Fe/Ti mixed map and the Fe/Ti intensity profile. The dots correspond to the experimental data, the black lines to the fitting curves.

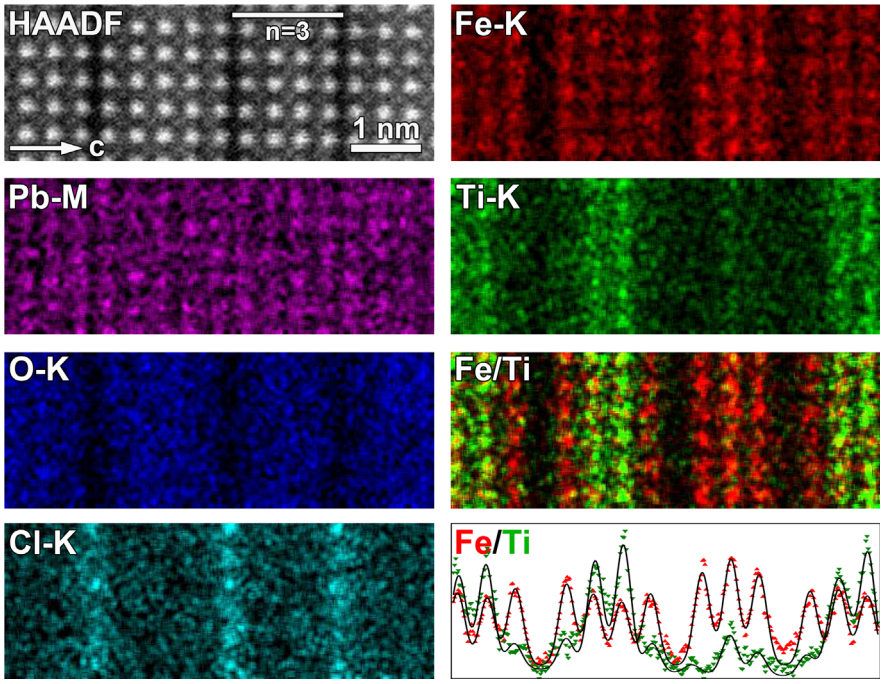

Fig. 11. High resolution HAADF-STEM image (upper corner) of the defect part of $Pb_5Fe_3TiO_{11}Cl$ taken along the [100] zone axis, individual Pb, Fe, Ti, O and Cl atomic EDX elemental maps, Fe/Ti mixed map and the Fe/Ti intensity profile. The dots correspond to the experimental data, the black lines to the fitting curves.

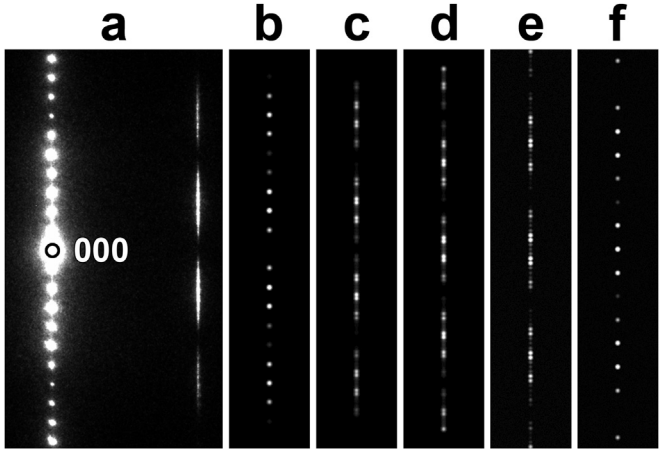

Fig. 12. Enlarged fragment of the ED pattern taken along the [310] zone (a) together with theoretical ED patterns calculated for the 5-fold supercell with the following alternation of cells with out-of-phase rotated (AB/BA) and in-phase rotated (AA/BB) octahedra: AB–AB–AB–AB–AB (b); AB–BA–AB–BA–AB (c); AA–BB–AA–BB–AA (d); AA–BB–AA–BB–BB (e); AA–AA–AA–AA–AA (f). The patterns have been calculated using the multislice method for a thickness of 10 nm.

$Sm_3Ti_3Se_2O_8$ [37], where Ti^{4+} is surrounded by five O atoms with similar Ti–O distances and one S or Se atom with much longer Ti–S/Se distance. In our study using a combination of NPD data and atomic resolution STEM-EDX measurements we have unambiguously demonstrated that the Fe^{3+}/Ti^{4+} ordering is not complete. This makes $Pb_5Fe_3TiO_{11}Cl$ an interesting example of a structure with Ti^{4+} in square-pyramidal oxygen coordination.

In $Pb_5Fe_3TiO_{11}Cl$, the FeTi1–O distance in the $(FeTi1)O_5$ pyramids is shorter for the apical O3 oxygen atom with $d(FeTi1–O3)=1.82$ Å, and longer for the basal O1 atoms with $d(FeTi1–O1)=2.03$ Å (all values in this paragraph are given for $T=300$ K). Whereas the (FeTi1–O1) distance is the same as in the $Pb_4Fe_3O_8Cl$ and $Pb_4BiFe_4O_{11}Cl$, the FeTi1–O3 distance is noticeably shorter (it is 1.88 Å for $Pb_4Fe_3O_8Cl$ [3,4] and 1.85 Å for $Pb_4BiFe_4O_{11}Cl$ [5]). The $(FeTi2)O_6$ octahedra are, on the contrary, more symmetrical in $Pb_5Fe_3TiO_{11}Cl$ than in $Pb_4BiFe_4O_{11}Cl$. The cations at the FeTi2 site are still displaced along the *c*-axis from the basal oxygen plane of the $FeTi2O_6$ octahedra toward the center of the perovskite block. However, the magnitude of the displacement is smaller. It is 0.1 Å in $Pb_4BiFe_4O_{11}Cl$ and only 0.05 Å in $Pb_5Fe_3TiO_{11}Cl$. As a result, the distances between FeTi2 and the apical oxygen atoms are $d(FeTi2–O3)=2.09$ Å and $d(FeTi2–O4)=2.00$ Å. The distance between FeTi2 and the basal O2 oxygen atom is 1.97 Å. For comparison, the corresponding values in $Pb_4BiFe_4O_{11}Cl$ are 2.20, 1.96 and 1.99 Å [5].

$Pb_4BiFe_4O_{11}Cl$ and $Pb_5Fe_3TiO_{11}Cl$ differ in the locally ordered rotation patterns of the $(FeTi2)O_6$ octahedra about the *c*-axis (the $(FeTi1)O_5$ pyramids do not rotate). The *P*4/*mmm* space group of $Pb_5Fe_3TiO_{11}Cl$ suggests a fully disordered octahedra rotation. However, the presence of the diffuse intensity streaks parallel to the c^* direction on the [310] ED pattern (see Fig. 3) indicates the presence of certain short-range ordered stacking sequences of the unit cells with in-phase and out-of-phase octahedra rotations. Possible scenarios were considered in the frame of the $a'=a\sqrt{2}$, $b'=b\sqrt{2}$, $c'=5c$ superstructure containing 10 octahedral layers, half of which are rotated clockwise (say, A) and another half is rotated counter-clockwise (say, B). One of the possibilities is if the octahedra have out-of-phase rotations in each subsequent unit cell resulting in the AB–AB–AB–AB–AB sequence. Another scenario is realized if the octahedra in one unit cell rotate in-phase (AA or BB), whereas the AA and BB unit cells alternate along the *c* direction as the AA–BB–AA–BB–AA sequence. Other more complex sequences can also be considered. To find out what is the most plausible pattern in $Pb_5Fe_3TiO_{11}Cl$, theoretical ED patterns have been calculated for the sequences AB–AB–AB–AB–AB, AB–BA–AB–BA–AB, AA–BB–AA–BB–AA, AA–BB–AA–BB–BB and AA–AA–AA–AA–AA. The comparison of the diffuse intensity modulation from the experimental ED pattern with the calculated intensities and positions of the satellites is shown in Fig. 12. One can notice that the sequences AB–AB–AB–AB–AB and AB–BA–AB–BA–AB reproduce best the experimentally observed intensity variation within the streaks. In other words, octahedra layers within one unit cell

clearly prefer the out-of-phase rotation. Violation of this sequence leads to the diffuse intensity on the experimental pattern instead of sharp dots as on the calculated patterns. In contrast to $Pb_5Fe_3TiO_{11}Cl$, in the $Pb_4BiFe_4O_{11}Cl$ structure the in-phase (AA or BB) octahedra rotation prevails, being locally violated with unit cells with out-of-phase rotations according to the most probable sequences AB–AA–AB–AA–AA and BA–AA–AB–AA–AA [5].

5. Conclusions

The perovskite-based oxychloride homologous series $A_{n+1}B_nO_{3n-1}Cl$ is expanded with a new $n=4$ member with a composition $Pb_5Fe_3TiO_{11}Cl$. The crystal structure of $Pb_5Fe_3TiO_{11}Cl$ consists of truncated quadruple perovskite blocks separated by Pb_2Cl slabs. In the perovskite blocks two layers of $(Fe,Ti)O_6$ octahedra are sandwiched between two layers of $(Fe,Ti)O_5$ square pyramids. Both octahedra and square pyramids are jointly occupied by Fe and Ti what makes this structure a rare example of Ti^{4+} in five-fold oxygen coordination environment. Below 450(10) K $Pb_5Fe_3TiO_{11}Cl$ is antiferromagnetically ordered with a G-type arrangement of the ordered Fe moments. The values of the ordered Fe magnetic moments at 1.5 K are 4.06(4) μ_B and 3.86(5) μ_B on the octahedral and square-pyramidal sites, respectively.

Acknowledgments

M.B., D.B. and J.H. acknowledge the funding from the Research Foundation – Flanders under grant number G.0184.09N. This work is partially based on experiments performed at the Swiss spallation neutron source SINQ, Paul Scherrer Institute, Villigen, Switzerland. Experimental support of Denis Sheptyakov (PSI) is kindly acknowledged.

Appendix A. Supporting information

Supporting data associated with this article can be found in the online version at http://dx.doi.org/10.1016/j.jssc.2014.04.002.

References

[1] R.C. Rouse, Am. Mineral. 56 (1971) 625.
[2] J. Emery, A. Cereze, F. Varret, J. Phys. Chem. Solids 41 (1980) 1035, http://dx.doi.org/10.1016/0022-3697(80)90056-6.
[3] J. Pannetier, P. Batail, J. Solid State Chem. 39 (1981) 15, http://dx.doi.org/10.1016/0022-4596(81)90297-8.
[4] C.S. Knee, M.T. Weller, J. Mater. Chem. 11 (2001) 2350, http://dx.doi.org/10.1039/b102092g.
[5] M. Batuk, D. Batuk, A.A. Tsirlin, M.G. Rozova, E.V. Antipov, J. Hadermann, G. Van Tendeloo, Inorg. Chem. 52 (2013) 2208, http://dx.doi.org/10.1021/ic302667a.
[6] R. Li, Inorg. Chem. 36 (1997) 4895, http://dx.doi.org/10.1021/ic970314w.
[7] R. Li, Phys. C: Supercond. 277 (1997) 252, http://dx.doi.org/10.1016/S0921-4534(97)00090-7.
[8] R. Li, J. Solid State Chem. 130 (1997) 154, http://dx.doi.org/10.1006/jssc.1996.7264.
[9] R.J. Crooks, C.S. Knee, M.T. Weller, Chem. Mater. 10 (1998) 4169, http://dx.doi.org/10.1021/cm980609n.
[10] A.C. Mclaughlin, J.A. McAllister, L.D. Stout, J.P. Attfield, Solid State Sci. 4 (2002) 431, http://dx.doi.org/10.1016/S1293-2558(02)01271-2.
[11] R.J. Cava, P. Bordet, J.J. Capponi, C. Chaillout, J. Chenavas, T. Fournier, E.A. Hewat, J.L. Hodeau, J.P. Levy, M. Marezio, B. Batlogg, L.W. Rupp, Phys. C: Supercond. 167 (1990) 67, http://dx.doi.org/10.1016/0921-4534(90)90487-Y.
[12] N.C. Hyatt, J.A. Hriljac, Phys. C: Supercond. 366 (2002) 283, http://dx.doi.org/10.1016/S0921-4534(01)00902-9.
[13] A.C. Mclaughlin, J.A. McAllister, L.D. Stout, J.P. Attfield, Phys. Rev. B 65 (2002) 8, http://dx.doi.org/10.1103/PhysRevB.65.172506.
[14] A.C. Mclaughlin, J.P. Attfield, R.S. Liu, L.-Y. Jang, W.Z. Zhou, J. Solid State Chem. 177 (2004) 834, http://dx.doi.org/10.1016/j.jssc.2003.09.016.
[15] A.M. Abakumov, M. Batuk, A.A. Tsirlin, O.A. Tyablikov, D.V. Sheptyakov, D.S. Filimonov, K.V. Pokholok, V.S. Zhidal, M.G. Rozova, E.V. Antipov, J. Hadermann, G. Van Tendeloo, Inorg. Chem. 52 (2013) 7834, http://dx.doi.org/10.1021/ic3026667.
[16] A.M. Abakumov, J. Hadermann, M. Batuk, H. D'Hondt, O.A. Tyablikov, M.G. Rozova, K.V. Pokholok, D.S. Filimonov, D.V. Sheptyakov, A.A. Tsirlin, D. Niermann, J. Hemberger, G. Van Tendeloo, E.V. Antipov, Inorg. Chem. 49 (2010) 9508, http://dx.doi.org/10.1021/ic101233s.
[17] P. Fischer, G. Frey, M. Koch, M. Konnecke, V. Pomjakushin, J. Schefer, R. Thut, N. Schlumpf, R. Bürge, U. Greuter, S. Bondt, E. Berruyer, Phys. B: Condens. Matter 276–278 (2000) 146, http://dx.doi.org/10.1016/S0921-4526(99)01399-X.
[18] J. Rodríguez-Carvajal, Phys. B: Condens. Matter 192 (1993) 55, http://dx.doi.org/10.1016/0921-4526(93)90108-I.
[19] C. Koch, Determination of Core Structure Periodicity and Point Defect Density along Dislocations, Arizona State University, Arizona, USA, 2002.
[20] J. Owen, J.H.M. Thornley, Rep. Prog. Phys. 29 (1966) 675, http://dx.doi.org/10.1088/0034-4885/29/2/306.
[21] B.C. Tofield, B.E.F. Fender, J. Phys. Chem. Solids 31 (1970) 2741, http://dx.doi.org/10.1016/0022-3697(70)90272-6.
[22] D. Sheptyakov, N.Z. Ali, M. Jansen, J. Phys.: Condens. Matter 22 (2010) 426001, http://dx.doi.org/10.1088/0953-8984/22/42/426001.
[23] D.P. Landau, Handbook of Magnetism and Advanced Magnetic Materials. Volume 1: Fundamentals and Theory, John Wiley & Sons, The University of Georgia, Athens, GA, USA, 2007.
[24] M.T. Dove, Am. Mineral. 82 (1997) 213.
[25] V.Y. Pomjakushin, A.M. Balagurov, T.V. Elzhov, D.V. Sheptyakov, P. Fischer, D. Khomskii, V. Yushankhai, A.M. Abakumov, M.G. Rozova, E.V. Antipov, M.V. Lobanov, S.J.L. Billinge, Phys. Rev. B 66 (2002) 184412, http://dx.doi.org/10.1103/PhysRevB.66.184412.
[26] H. Keller, W. Kündig, H. Arend, Le J. Phys. Colloq. 37 (1976) C6-629, http://dx.doi.org/10.1051/jphyscol:19766131.
[27] M. Wojdyr, J. Appl. Crystallogr. 43 (2010) 1126, http://dx.doi.org/10.1107/S0021889810030499.
[28] M. Anderson, K. Greenwood, G. Taylor, K.R. Poeppelmeier, Prog. Solid State Chem. 22 (1993) 197, http://dx.doi.org/10.1016/0079-6786(93)90004-B.
[29] G. King, P.M. Woodward, J. Mater. Chem. 20 (2010) 5785, http://dx.doi.org/10.1039/b926757c.
[30] P.B. Moore, J. Louisnathan, Science 156 (1967) 1361, http://dx.doi.org/10.1126/science.156.3780.1361.
[31] T. Hoche, C. Rüssel, W. Neumann, Solid State Commun. 110 (1999) 651, http://dx.doi.org/10.1016/S0038-1098(99)00145-3.
[32] M.A. Roberts, G. Sankar, J.M. Thomas, R.H. Jones, H. Du, J. Chen, W. Pang, R. Xu, Nature 381 (1996) 401, http://dx.doi.org/10.1038/381401a0.
[33] R. Werthmann, R. Hoppe, Z. Anorg. Allg. Chem. 523 (1985) 54, http://dx.doi.org/10.1002/zaac.19855230408.
[34] C. Weiss, R. Hoppe, Z. Anorg. Allg. Chem. 621 (1995) 1447, http://dx.doi.org/10.1002/zaac.19956210902.
[35] R.D. Aughterson, G.R. Lumpkin, M.D.L. Reyes, N. Sharma, C.D. Ling, B. Gault, K.L. Smith, M. Avdeev, J.M. Cairney, J. Solid State Chem. 213 (2014) 182, http://dx.doi.org/10.1016/j.jssc.2014.02.029.
[36] M. Goga, R. Seshadri, V. Ksenofontov, P. Gütlich, W. Tremel, Chem. Commun. 5 (1999) 979, http://dx.doi.org/10.1039/a809737b.
[37] V. Meignen, C. Deudon, A. Lafond, C. Boyer-Candalen, A. Meerschaut, Solid State Sci. 3 (2001) 189, http://dx.doi.org/10.1016/S1293-2558(00)01130-4.